## Journal of Materials Chemistry A



**PAPER** 

View Article Online



Cite this: DOI: 10.1039/d4ta03045a

# Fluorescence-enhanced light-blue bilayer radiative cooling coatings†

Xue Ma,<sup>a</sup> Yang Fu,<sup>a</sup> Ning Yang,<sup>b</sup> Xin Hu,<sup>c</sup> Jian-Guo Dai,<sup>b</sup> Bin Fei<sup>c</sup> and Dangyuan Lei (1) \*\*a

Daytime passive radiative cooling devices expel heat into the cold outer space by thermal radiation, offering an energy-efficient strategy for cooling terrestrial objects. Colored coolers are more desirable than white ones in real-world applications under the demands of aesthetics and reducing light pollution. The recently proposed fluorescence-assisted methods based on phosphor powders have simultaneously achieved sub-ambient cooling performance and bright colors, ascribed to the fluorescence-induced heat gain offset and consequent high-effective solar reflectance. However, the color gamut of radiative coolers is still limited due to the lack of blue colors, attributed to the absorption of the majority of visible light. In this work, we propose and prepare a light-blue radiative cooling coating composed of a  $\rm ZrO_2$  white bottom layer with a remarkable high solar reflectance of >98% and an ultra-thin top layer consisting of a blue phosphor ( $\rm SrO\cdot Al_2O_3$ : Eu). This bilayer coating reveals a high effective solar reflectance of 94% with a vivid light-blue appearance and achieves a sub-ambient temperature reduction of 3–4.4 °C under a peak solar intensity of >800 W m<sup>-2</sup> and an average humidity of 30% in Hong Kong. Our work paves the way for fabricating highly efficient radiative cooling coatings with a whole gamut of tunable colors.

Received 2nd May 2024 Accepted 5th July 2024

DOI: 10.1039/d4ta03045a

rsc.li/materials-a

#### Introduction

The current vapor compression-based cooling technologies have contributed to aggravating the global energy crisis and the global warming effect due to their massive energy consumption, leading to much interest in improving the efficiency of the existing cooling systems and pursuing new alternative cooling technologies.<sup>1-8</sup> Recently, passive daytime radiative cooling has attracted worldwide interest due to its potential for cooling consumption and greenhouse emission.<sup>2,4,5,9-14</sup> Considering the negligible blackbody radiation in the outer space at an extremely low temperature of 2.7 K, radiative cooling surfaces can utilize the outer space as a heatsink and cool-down terrestrial objects through infrared thermal emission in the atmosphere window (8-13 µm).<sup>3,4,9</sup> Achieving a sub-ambient cooling effect during the daytime requires extremely low absorptivity in the highly intensive solar

Colored radiative cooling materials have been investigated to address the above-mentioned issues; however, the colorationinduced heat gain hinders the full exploitation of their radiative cooling potential.16-18 Various strategies and materials, exploiting color pigments, structural colors, and fluorescence materials, have been proposed for achieving sub-ambient colored radiative cooling coatings.5,16,19,20 Traditional color pigments can be easily integrated with the radiative cooling matrix, making them well-suited for commercialization in fullspectrum colored cooling coatings.5,16,21 However, the color stems from the reflected visible light while the remaining parts are absorbed. Introducing a traditional color pigment into a cooling coating thereby leads to inherent light absorption, particularly across the visible spectrum, resulting in unflavored solar heating.17 Structural coloration can reconfigure the reflected light spatially, i.e., decompose the visible light through varying the spectral reflection at different angles, with minimal light absorption and reduced solar heating, thereby unleashing the cooling capacity.<sup>20,22-29</sup> However, such structural colorations rely on complicated photonic structures and a complex nanofabrication process, which present difficulties in achieving costeffective large-scale production. 20,30-32 To balance the coloration

spectrum (0.3–2.5  $\mu$ m) and high emissivity in the infrared region, preferably within the atmospheric window.<sup>2</sup> Therefore, a white appearance with high solar reflectance is always employed to maximize the daytime cooling performance, which is visually harmful and aesthetically boring.<sup>2,4,9,15</sup>

<sup>\*</sup>Department of Materials Science and Engineering, Centre for Functional Photonics, and Hong Kong Branch of National Precious Metals Material Engineering Research Centre, City University of Hong Kong, 83 Tat Chee Avenue, Kowloon, Hong Kong, 999077, China. E-mail: dangylei@cityu.edu.hk

<sup>&</sup>lt;sup>b</sup>Department of Architecture and Civil Engineering, City University of Hong Kong, 83 Tat Chee Avenue, Kowloon, Hong Kong, 999077, China

School of Fashion and Textiles, The Hong Kong Polytechnic University, Hung Hom, Kowloon, Hong Kong, 999077, China

Published on 05 July 2024. Downloaded by City University of Hong Kong Library on 7/22/2024 12:43:04 PM

and cooling capacity for colored radiative cooling coatings, integrating fluorescence materials has been revealed as an alternative approach since they can re-emit the absorbed light as photons with longer wavelengths. 31,33-36 In addition, it can be well dispersed into the radiative cooling coating and maintain good optical properties, which make it highly compatible with current coating manufacturing processes. According to previous studies on colored radiative cooling based on fluorescence materials, versatile colors, such as yellow, green, and red, have been achieved and have exhibited sub-ambient cooling performance. 1,33,34 However, a blue sub-ambient cooling coating has not been realized yet since producing blue color requires the absorption of a larger amount of visible light. The absence of a blue coating limits the full-spectrum tunable coloration.

In this work, we propose a novel approach to address the limitation of the color variety in fluorescent-assisted colored radiative cooling coatings. By incorporating the blue phosphor  ${\rm SrO\cdot Al_2O_3}$ : Eu into an ultra-thin top layer, we aimed to achieve a vivid light-blue color while maintaining a high solar reflectance and infrared emissivity. Additionally, a  ${\rm ZrO_2}$  white bottom layer with extremely high solar reflectance was used to maximize the cooling efficiency of the coatings. The colored coating developed in this study demonstrated a high total solar reflectance of 94% with vivid light-blue color and achieved a remarkable sub-ambient temperature reduction larger than 3 °C in Hong Kong. This study paves the way for the fabrication of highly efficient radiative cooling coatings with tunable colors across the entire gamut.

#### Results and discussions

In general, the fundamental thermal processes involved in a typical daytime radiative cooling device at temperature T can be grouped into four sources, as expressed in eqn (1) below:

$$P_{\text{cool}}(T) = P_{\text{rad}}(T) - P_{\text{sun}} - P_{\text{atm}} - P_{\text{cond+conv}}$$
(1)

where  $P_{\rm rad}(T)$ ,  $P_{\rm sun}$ , and  $P_{\rm atm}$  are the outgoing thermal radiation power, absorbed solar irradiance, and absorbed atmospheric longwave radiation power by the device, respectively, and  $P_{\rm cond+conv}$  is the received heat convection and conduction from the surrounding environment. For colored radiative cooling coatings, most colored pigments can significantly absorb visible light and convert it to non-radiative thermal energy. However, higher color saturation would increase  $P_{\rm sun}$  and compromise the cooling effect. Regarding this issue, a fluorescent-assisted method is proposed to reduce solar absorption and solve the dilemma of colored radiative cooling. As shown in Fig. 1a, beyond the reflected sunlight as the counterparts of  $P_{\rm sun}$ , fluorescent materials could introduce an additional light emission channel toward the atmosphere.

As shown in Fig. 1b, previous studies on fluorescent colored radiative cooling coatings have been able to exhibit vivid colors and achieve a sub-ambient cooling effect. However, radiative cooling coatings based on blue fluorescence are still at the theoretical stage. The obstacle to obtaining blue sub-

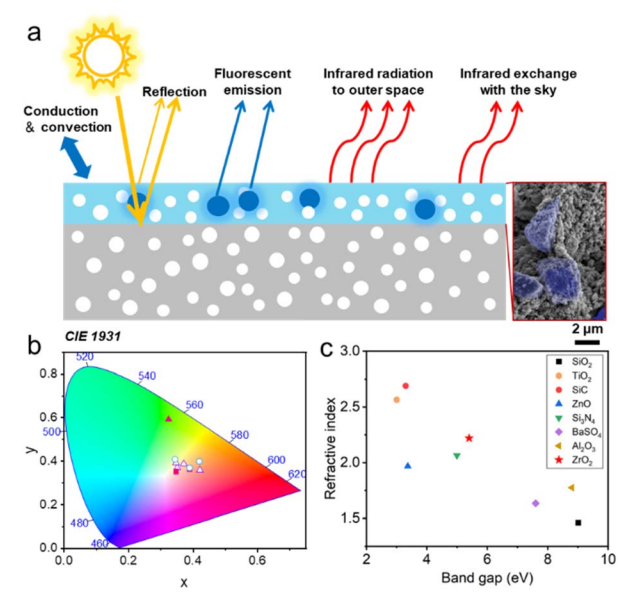


Fig. 1 (a) Schematic of the designed cooling coating and cooling mechanism. (b) CIE 1931 chromaticity coordinates in previous works on fluorescent colored sub-ambient cooling coatings. (The different signs correspond to different works. Reference: red triangle,¹ white triangle,³ red square,³ white circle³4,³8). (c) Refractive index over the band gap of some commonly used dielectric particles with a high refractive index.³9

ambient coatings is that a large amount of visible light will be absorbed for coloration, where the visible light counts for almost half of the solar energy.40 Two requirements should be satisfied to overcome the above obstacle: fluorescent pigments are needed to minimize the solar heat gain by coloration and an ultra-white base is needed to prevent excessive solar absorption. For the top-colored layer, we can see from the SEM images in Fig. 1a and S1† that the blue phosphor microparticles are uniformly dispersed in the polymer and surrounded by the monodispersed nanoparticles. While for the base layer, a higher refractive index of the nanoparticle is more favorable since the large dielectric contrast with the matrix leads to a stronger scattering of individual particles, resulting in greater reflection.39 Moreover, the band gap of the particle should be wider than 5 eV to avoid UV absorption. According to the summarized refractive index and band gap of some commonly used dielectric particles in Fig. 1c, ZrO2 nanoparticles were selected to be added as a filler.

As discussed above, before integrating fluorescent materials, a bilayer structure composed of a super-white bottom layer providing strong solar reflection and a thin top layer for coloration while suppressing near-infrared absorption was adopted. Fig. 2a illustrates the calculated scattering efficiency map for ZrO<sub>2</sub> nanoparticles of various diameters embedded in a polymer matrix. It is evident that larger ZrO<sub>2</sub> nanoparticles were more effective at scattering light at longer wavelengths. The scattering spectra of the ZrO<sub>2</sub> nanoparticles with different diameters are shown in Fig. S2.† Specifically, ZrO<sub>2</sub> nanoparticles with a diameter of 500 nm exhibited the highest scattering efficiency

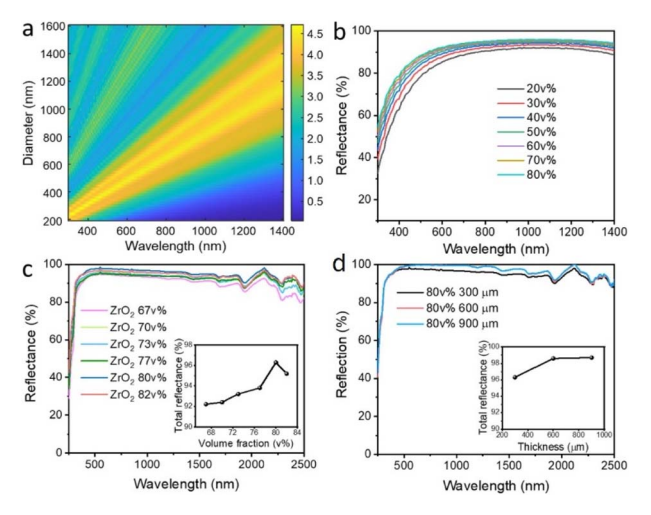


Fig. 2 (a) Stimulated scattering efficiency map of ZrO<sub>2</sub> nanoparticles with varied diameters and the solar intensity spectrum. (b) Calculated reflectance spectra of coatings encapsulating ZrO<sub>2</sub> nanoparticles using a Monte Carlo method. The diameter distribution of ZrO<sub>2</sub> nanoparticles is shown in Fig. S3.† (c) Measured reflectance spectra of polymer coatings with varying volume fractions of ZrO<sub>2</sub> nanoparticles. Inset is the corresponding total solar reflectance. (d) Measured reflectance spectra of ZrO2-based white coatings with different thicknesses. Inset is the corresponding total solar reflectance.

in the 500-1000 nm wavelength range, which covers the most energy-intensive region in the solar spectrum. Broadening the size distribution centered at ~500 nm would further increase the reflectance through the whole solar spectrum. After uniformly dispersing ZrO2 nanoparticles in water, the size distribution could be identified. As depicted in Fig. S3,† their average diameter was approximately 480 nm. Based on the size distribution and optical properties of both the fillers and matrix, a Monte Carlo method was utilized to calculate the reflectance spectra of the bottom coating under different volume fractions of ZrO2. As shown in Fig. 2b, the reflectance of the coatings increased as the volume fraction increased and approached saturation when the volume fraction was 70-80 v%. Guided by the calculation results, coatings with the same thickness but varied volume fractions (67 v%, 70 v%, 73 v%, 77 v%, 80 v%, and 82 v%) were fabricated. As shown in Fig. 2c, the experimental measurements revealed similar trends for the spectral reflectance as the calculation results. The inset shows the variation of the overall solar reflectance of the fabricated coatings, indicating a notable increase with the rising volume fraction of ZrO2 nanoparticles. A plateau could be observed at the volume fraction of 80%. Fig. 2d shows the reflectance spectra of the coatings with a ZrO<sub>2</sub> nanoparticles volume fraction of 80% but different thicknesses. The inset illustrates the variation of the overall solar reflectance with the thickness. It could be observed that beyond a coating thickness of 600 µm, the reflectance was stabilized at ~98.7% and did not further increase.

Next, the blue phosphor SrO·Al<sub>2</sub>O<sub>3</sub>: Eu was employed as the colored fluorescent material. Its excitation and emission spectra in Fig. 3a indicate that SrO·Al<sub>2</sub>O<sub>3</sub>: Eu could be excited by light of

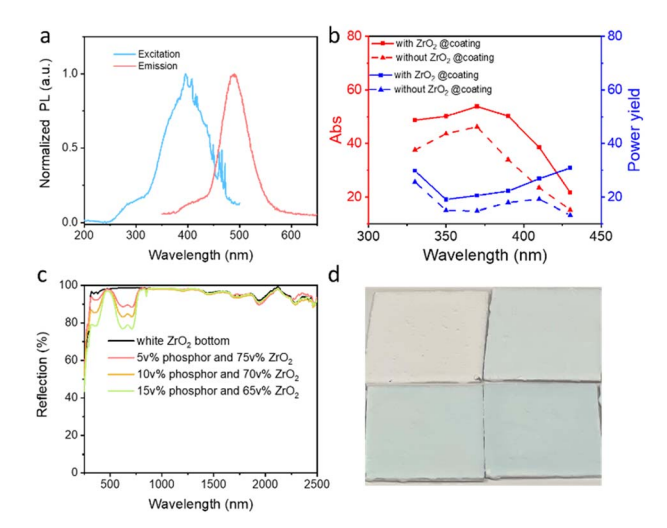


Fig. 3 (a) Excitation and emission spectra of the SrO·Al<sub>2</sub>O<sub>3</sub>: Eu blue phosphor. (b) Absorption and power yield spectra of the blue phosphor with (solid lines) and without (dashed lines) the ZrO<sub>2</sub> nanoparticles. (c) Reflectance spectra and (d) corresponding optical graphs of the bottom white coating and bilayer light-blue coatings with varied volume fractions of blue phosphor and ZrO2 nanoparticles. All the samples had the same total solid volume fraction of 80 v%.

around 400 nm, subsequently emitting light at longer wavelengths. Notably, the small Strokes shift of ~100 nm, indicating the minimal energy loss. Generally, the power intensity of fluorescent emission is much lower than the directly reflected sunlight and contributes less to the color presentation, ascribed to two main factors: one is that the excitation light is typically located in the short wavelength range, which accounts for only a limited portion of total solar power; and the other is the energy loss induced by the Stokes shift and non-unity quantum yield, which, fortunately, can be mitigated through a Purcell enhancement within the coating. 41,42 Therefore, to evaluate the influence on the fluorescence properties of phosphors when integrated into the coatings, the absorption of excitation light (Abs) and the power yield (PY) were investigated, which are defined as follows:

$$Abs = \int_{\lambda_{av, min}}^{\lambda_{ex, max}} hc \frac{I_{ref}(\lambda) - I_{PL}(\lambda)}{\lambda I_{ref}(\lambda)}$$
 (2)

$$PY = \frac{\int_{\lambda_{\text{em, min}}}^{\lambda_{\text{em, min}}} hc \frac{I_{\text{PL}}(\lambda) - I_{\text{ref}}(\lambda)}{\lambda}}{\int_{\lambda_{\text{ex, min}}}^{\lambda_{\text{ex, max}}} hc \frac{I_{\text{ref}}(\lambda) - I_{\text{PL}}(\lambda)}{\lambda}}{\lambda}}$$
(3)

where  $\lambda_{\rm ex,\ min} \sim \lambda_{\rm ex,\ max}$  and  $\lambda_{\rm em,\ min} \sim \lambda_{\rm em,max}$  are the wavelength range of excitation and emission of the phosphors,  $I_{PL}(\lambda)$  and  $I_{\text{ref}}(\lambda)$  are the measured photon intensity with and without the samples, and h and c are Planck's constant and the speed of light, respectively. As shown in Fig. 3b, the absorptions of excitation light increased by 6.5-16.3%, which was attributed to the electric field modification of the Mie resonators (i.e. ZrO<sub>2</sub> nanoparticles). The power yield represents the energy efficiency of radiative photon conversion and was increased by 4.0–17.6%. These improved photoluminescence properties indicate that

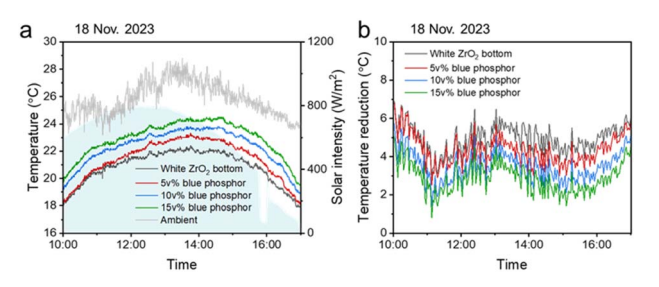


Fig. 4 (a) Recorded temperature curves of ambient air (grey), a single-layer  $\rm ZrO_2$  coating (black), and three bilayer light-blue coatings with phosphor volume fractions of 5 v% (red), 10 v% (blue), and 15 v% (green). (b) Temperature reduction of blue coatings with the phosphor volume fractions of 5 v% (red), 10 v% (blue), and 15 v% (green).

more light within the excitation range could be converted to longer wavelengths, leading to a higher potential for color reconfiguration.

The bilayer blue coatings consisted of an ultra-white bottom layer and a  ${\sim}25~\mu m$  top layer with a varied blue phosphor volume fraction (5 v%, 10 v%, and 15 v%). All the samples had the same total solid volume fraction of 80 v%, since a higher solid concentration could cause the coatings to crack. As shown in Fig. 3c and Table S1,† the reflectances of the white coating and the unexcited fluorescent blue coatings with a varied blue phosphor volume fraction (5 v%, 10 v%, and 15 v%) were 97.6%, 94.1%, 91.5%, and 88%, respectively. The reflectance exhibited a progressive decline in reflectivity with the increase in blue phosphor concentration, a phenomenon attributable to the intrinsic light absorption of the phosphor. The corresponding photos of the coatings are shown in Fig. 3d.

In an outdoor field test conducted under clear blue skies in Hong Kong, we evaluated the cooling capacity of bilayer-colored cooling coatings (Fig. S6†). Fig. 4a shows the temperature variations of these coatings compared to the ambient temperature recorded under a clear sky with a peak solar irradiance >800 W m<sup>-2</sup>. The wind speed and the humidity during the measurements are shown in Fig. S7.†

As illustrated in Fig. 4b, the white  $\rm ZrO_2$  bottom layer demonstrated a notable cooling effect, reducing the surface temperature by 5.2 °C relative to the ambient temperature. In contrast, the bilayer blue coatings, incorporating blue phosphor concentrations of 5 v%, 10 v%, and 15 v%, showed a gradational decrease in cooling efficiency with increasing phosphor content. Specifically, temperature reductions of 4.4 °C, 3.5 °C, and 3.0 °C were observed for the respective phosphor concentrations (Fig. 4b).

## Experimental

#### **Materials**

 $SrO \cdot Al_2O_3$ : Eu was purchased from Guangzhou Chuangrong Chemical Technology Co. Ltd. The polystyrene-acrylic matrix was purchased from BASF Co. Ltd. Polycarboxylate sodium salt was employed as the dispersant agent. Polyurethane associative served as the suspending agent. The anti-foaming agent was

mineral oil. The film-forming agent was 9Z-dodecenyl acetate, and the leveling agent was polyurethane. All the agents were purchased from Guang Zhou Run Hong Chemical.

#### Sample preparation

The preparation of the white coating proceeded as follows: 20 v% polystyrene-acrylic emulsion,  $80 \, \text{v}\% \, \text{ZrO}_2$  nanoparticles, and an appropriate amount of water were first mixed in a 50 ml beaker with continuous stirring, followed by the addition of the dispersant agent, suspending agent, and leveling agent. The mixture was stirred at 1200 rpm for 1 h. Then the stirring speed was turned down to 400 rpm, and 0.4 g anti-foaming agent and 1 g film-forming agent were added. After 30 min of stirring, the mixture was sprayed evenly on a cement board with a spray gun under a pressure of 5 MPa.

The preparation of the fluorescent blue top layer proceeded as follows: 20 v% polystyrene-acrylic emulsion, 75 v%  $\rm ZrO_2$  microparticles, 5 v% phosphor, and an appropriate amount of water were first mixed in a 50 ml beaker under continuous stirring conditions, followed by the addition of the dispersant agent, suspending agent, and leveling agent. The mixture was stirred at 1200 rpm for 1 h. Then, the stirring speed was turned down to 400 rpm, and 0.4 g anti-foaming agent and 1 g filmforming agent were added. After 30 min of stirring, the mixture was sprayed evenly on a cement board with a spray gun under a pressure of 5 MPa.

#### Sample characterization and field tests

The reflectance spectra of the coatings were measured on a PerkinElmer Lambda 1050+ UV/VIS/NIR Wide Band Spectrometer equipped with an integrating sphere. The particle-size distribution was measured using a Malvern Zetasizer Nano S (ZEN1600) particle analyzer. The excitation spectra, emission spectra, PL lifetime, and quantum yield of the pure phosphors/ fluorescent cooling coatings were collected on an Edinburgh Instruments FLS980 fluorescence spectrometer. The infrared emissivity of the cooling coatings was measured using a transform infrared spectrometer (FT-IR Spectrometer, Spectrum 100, PerkinElmer) with a diffuse gold integrating sphere. The scanning range was 650-4000 cm<sup>-1</sup> at a resolution of 4 cm<sup>-1</sup>, and a total of 16 scans were collected. The real-time temperature of the coatings was recorded on a MEMORY HiLOGGER LR8431-30 multichannel temperature collector with K-type thermocouples. The thermocouple for detecting the ambient temperature was positioned inside a light-shielded white louvered box. The solar intensity and relative humidity were recorded by an accurate pyranometer (EKO MS-802) and a mini weather station.

#### Scattering efficiency calculations

The scattering efficiency map in Fig. 2a was calculated for spherical ZrO<sub>2</sub> particles in the polymer. At each diameter of ZrO<sub>2</sub>, we calculated the spectral scattering efficiency with the Mie formula that solves Maxwell's equation. The refractive indices of the polymer and ZrO<sub>2</sub> were obtained from our previous measurements<sup>41</sup> and from previous work,<sup>43</sup>

respectively. We have added corresponding statements about this in the "Experimental" section.

#### Conclusions

In this study, we introduced an innovative strategy to enhance the color diversity of fluorescent-assisted, colored radiative cooling coatings. Our approach involved integrating a blue phosphor, specifically SrO·Al<sub>2</sub>O<sub>3</sub>: Eu, into an ultra-thin top layer. This integration was aimed at producing a vibrant color effect while ensuring high solar reflectance and infrared emissivity. To augment the cooling efficiency, we utilized a ZrO<sub>2</sub> white bottom layer, known for its exceptionally high solar reflectance. The colored coating exhibited a remarkable total solar reflectance of 94% and displayed a distinctively vivid coloration. Furthermore, the coating demonstrated significant temperature-reduction capabilities under hot and humid climate conditions, achieving a notable sub-ambient temperature decrease of 3-4.4 °C. This work represents a significant step forward in the development of highly efficient radiative cooling coatings, offering tunability in color across the full spectrum.

### Data availability

The data supporting this article have been included as part of the ESI.†

#### Author contributions

Xue Ma: conceptualization, investigation, and writing. Yang Fu: investigation. Ning Yang: investigation. Xin Hu: investigation. Jian-Guo Dai: supervision. Bin Fei: investigation. Dangyuan Lei: conceptualization and supervision.

#### Conflicts of interest

There are no conflicts to declare.

## Acknowledgements

We acknowledge the financial support by the City University of Hong Kong through the ARG project (9667246), the Research Grants Council of Hong Kong through a GRF project (15223120) and a CRF project (C5051-22GF), the Innovation and Technology Commission of Hong Kong through an ITF grant (MHP/ 162/22), the Centre for Functional Photonics of the City University of Hong Kong, and the Hong Kong Branch of National Precious Metals Material Engineering Research Centre (ITC Fund).

#### Notes and references

- 1 D. Chae, S. Y. Lee, H. Lim, S. Son, J. Ha, J. Park, J. H. Park, S. J. Oh and H. Lee, ACS Appl. Mater. Interfaces, 2023, 15, 58274-58285.
- 2 D. Zhao, A. Aili, Y. Zhai, S. Xu, G. Tan, X. Yin and R. Yang, Appl. Phys. Rev., 2019, 6, 021306.

- 3 M. M. Hossain and M. Gu, Adv. Sci., 2016, 3, 1500360.
- 4 B. Zhao, M. Hu, X. Ao, N. Chen and G. Pei, Appl. Energy, 2019, 236, 489-513.
- 5 Z. Ding, X. Li, X. Fan, M. Xu, J. Zhao, Y. Li and H. Xu, Carbon Capture Sci. Technol., 2022, 4, 100066.
- 6 R. Pacheco, J. Ordóñez and G. Martínez, Renewable Sustainable Energy Rev., 2012, 16, 3559-3573.
- 7 J. P. Bijarniya, J. Sarkar and P. Maiti, Renewable Sustainable Energy Rev., 2020, 133, 110263.
- 8 B. I. Cook, J. E. Smerdon, R. Seager and S. Coats, Clim. Dyn., 2014, 43, 2607-2627.
- 9 X. Yu, J. Chan and C. Chen, Nano Energy, 2021, 88, 106259.
- 10 J. Liu, Z. Zhou, J. Zhang, W. Feng and J. Zuo, Mater. Today Phys., 2019, 11, 100161.
- 11 A. P. Raman, M. A. Anoma, L. Zhu, E. Rephaeli and S. Fan, Nature, 2014, 515, 540-544.
- 12 J. Siecker, K. Kusakana and E. B. Numbi, Renewable Sustainable Energy Rev., 2017, 79, 192-203.
- 13 S. Ahmed, Z. Li, M. S. Javed and T. Ma, Mater. Today Energy, 2021, 21, 100776.
- 14 X. Lu, P. Xu, H. Wang, T. Yang and J. Hou, Renewable Sustainable Energy Rev., 2016, 65, 1079-1097.
- 15 M. Zeyghami, D. Y. Goswami and E. Stefanakos, Sol. Energy Mater. Sol. Cells, 2018, 178, 115-128.
- 16 W. Xi, Y. Liu, W. Zhao, R. Hu and X. Luo, Int. J. Therm. Sci., 2021, 170, 107172.
- 17 B. Xie, Y. Liu, W. Xi and R. Hu, Mater. Today Energy, 2023, 101302.
- 18 R. A. Yalçın, E. Blandre, K. Joulain and J. Drévillon, ACS photonics, 2020, 7, 1312-1322.
- 19 S. Yu, Q. Zhang, Y. Wang, Y. Lv and R. Ma, Nano Lett., 2022, 22, 4925-4932.
- 20 J. Zhao, F. Nan, L. Zhou, H. Huang, G. Zhou, Y.-f. Zhu and Q. Ou, Sol. Energy Mater. Sol. Cells, 2023, 251, 112136.
- 21 H.-D. Wang, C.-H. Xue, C.-Q. Ma, X.-X. Jin, M.-C. Huang, Y.-G. Wu, S.-Q. Lv, A.-J. Chang, J. Li and X.-J. Guo, ACS Sustain. Chem. Eng., 2024, 4, 1681-1693.
- 22 T. Suichi, A. Ishikawa, Y. Hayashi and K. Tsuruta, Proc. SPIE, 2017, 10369, 35-40.
- 23 S. Ishii, D. Hernández-Pinilla, N. K. Tanjaya and T. Nagao, Sol. Energy Mater. Sol. Cells, 2023, 259, 112463.
- 24 D. Chae, M. Kim, P.-H. Jung, S. Son, J. Seo, Y. Liu, B. J. Lee and H. Lee, ACS Appl. Mater. Interfaces, 2020, 12, 8073-8081.
- 25 W. Li, Y. Shi, K. Chen, L. Zhu and S. Fan, ACS Photonics, 2017, 4, 774-782.
- 26 X. Wang, X. Liu, Z. Li, H. Zhang, Z. Yang, H. Zhou and T. Fan, Adv. Funct. Mater., 2020, 30, 1907562.
- 27 H. Zhang, K. C. Ly, X. Liu, Z. Chen, M. Yan, Z. Wu, X. Wang, Y. Zheng, H. Zhou and T. Fan, Proc. Natl. Acad. Sci., 2020, 117, 14657-14666.
- 28 H. H. Kim, E. Im and S. Lee, Langmuir, 2020, 36, 6589-6596.
- 29 M. Lee, G. Kim, Y. Jung, K. R. Pyun, J. Lee, B.-W. Kim and S. H. Ko, Light: Sci. Appl., 2023, 12, 134.
- 30 M. Qian, Q. Shi, L. Qin, J. Huang, C. Guo, Y. Liu and K. Yu, Photonics, 2023, 10, 645.
- 31 R. A. Yalçın, E. Blandre, K. Joulain and J. Drévillon, J. Photonics Energy, 2021, 11, 032104.

- 32 H. Xia and C. Fan, Sol. Energy Mater. Sol. Cells, 2024, 266, 112693.
- 33 J. Xu, R. Wan, W. Xu, Z. Ma, X. Cheng, R. Yang and X. Yin, *Mater. Today Nano*, 2022, **19**, 100239.
- 34 X. Wang, Q. Zhang, S. Wang, C. Jin, B. Zhu, Y. Su, X. Dong, J. Liang, Z. Lu and L. Zhou, *Sci. Bull.*, 2022, **67**, 1874–1881.
- 35 P. Berdahl, S. S. Chen, H. Destaillats, T. W. Kirchstetter, R. M. Levinson and M. A. Zalich, *Sol. Energy Mater. Sol. Cells*, 2016, 157, 312–317.
- 36 S. Min, S. Jeon, K. Yun and J. Shin, *ACS Photonics*, 2022, 9, 1196–1205.
- 37 S. Son, S. Jeon, D. Chae, S. Y. Lee, Y. Liu, H. Lim, S. J. Oh and H. Lee, *Nano Energy*, 2021, **79**, 105461.

- 38 X. Ma, Y. Fu, D. Liu, N. Yang, J. G. Dai and D. Lei, *Adv. Opt. Mater.*, 2024, 2303296.
- 39 P. Li, A. Wang, J. Fan, Q. Kang, P. Jiang, H. Bao and X. Huang, *Adv. Funct. Mater.*, 2022, 32, 2109542.
- 40 J. Mandal, Y. Fu, A. C. Overvig, M. Jia, K. Sun, N. N. Shi, H. Zhou, X. Xiao, N. Yu and Y. Yang, *Science*, 2018, 362, 315–319.
- 41 X. Ma, Y. Fu, A. Portniagin, N. Yang, D. Liu, A. L. Rogach, J.-G. Dai and D. Lei, *J. Mater. Chem. A*, 2022, **10**, 19635–19640.
- 42 X. Xue, M. Qiu, Y. Li, Q. Zhang, S. Li, Z. Yang, C. Feng, W. Zhang, J. G. Dai and D. Lei, *Adv. Mater.*, 2020, 32, 1906751.
- 43 D. L. Wood and K. Nassau, Appl. Opt., 1982, 21, 2978-2981.